

Development a new positron source for spin-polarized positron beam generation

Masaki Maekawa^a, Ken Wada^a, Atsuo Kawasuso^a

^a National Institutes for Quantum and Radiological Science and Technology, 1233 Watanuki, Takasaki, Gunma 370-1292, Japan



ARTICLE INFO

Keywords:

Slow positron beam
Spin polarized
²²Na source

ABSTRACT

A sealed positron source that can sufficiently reduce the backscattered component was fabricated using an aqueous ²²NaCl solution and a graphite backing material. The spin polarization of the emitted positrons was evaluated as 39%, which was 1.7 times higher than that of a commercial source with a heavy-metal backing material. This source increased the amplitude of the magnetic Doppler broadening spectrum for ferromagnetic iron.

1. Introduction

Spin-polarized positron-annihilation spectroscopy (SP-PAS) is a powerful technique for evaluating electron spin polarization at the surface, interface, and in the bulk [1–8]. Because the pair-annihilation probability of a positron and an electron depends on their relative spin direction, the positron–electron momentum distribution shows asymmetry upon spin reversal. We have demonstrated that the Doppler broadening of annihilation radiation (DBAR) technique with spin-polarized positrons can be used for studying ferromagnetic materials [9–11]. For example, because positrons are preferentially trapped in atomic vacancies, the SP-PAS method can detect the electron spins localized therein that may be the origin of the vacancy-induced magnetism [12,13]. In addition, spin-polarized surface positronium spectroscopy can be used to investigate the spin-polarized electronic states of the first surface layer [14–17].

For better SP-PAS experiments, a highly spin-polarized positron beam is required. Positrons emitted from radioisotope sources are longitudinally spin-polarized due to the parity non-conservation in the weak interaction [18–20]. The longitudinal spin polarization of positrons emitted at an open angle, α , is given by $P_{\pm} = (v/c)(1 + \cos\alpha)/2$, where v and c are the speeds of positrons and light, respectively [21]. Hence, to increase the positron spin polarization, α should be restricted. However, normally, α is greater than 90° due to the inclusion of backscattered positrons from the backing material [22–25]. Consequently, the total spin polarization of emitted positrons is degraded.

In this work, to obtain highly spin-polarized positrons, we developed a positron source using graphite as a backing material that can suppress the backscattered component compared with heavy metals used in commercial sources. Graphite also has superior corrosion and

radiation resistance. The positron spin-polarization of the highly spin-polarized (HSP) source was 1.7 times greater than that of a conventional commercial (CONV) source [25].

2. Source design and fabrication

Fig. 1 shows a schematic of the source structure. A commercially available aqueous ²²NaCl solution was deposited on a graphite backing material. To avoid the precipitation of a ring of NaCl, a tapered hole with a bottom diameter of $\phi 2$ mm, an entrance diameter of $\phi 2.5$ mm, and a depth of 1 mm was fabricated. Furthermore, fine patterns were scratched on the bottom surface.

For radiation protection, the ²²NaCl solution was deposited by an automatic remote-controlled syringe pump (Fig. 2). A 1 μ L spherical droplet was formed at the tip of the syringe (100 μ L). The graphite backing material was lifted to the droplet until they touched. The stage was moved down until the droplet was separated from the syringe tip. After the droplet was completely dried, the next drop was deposited. In total, 220 μ L (296 MBq) aqueous solution was deposited. To shorten the drying time, the graphite backing material was heated to 60 $^{\circ}$ C by a ceramic heater. The active area was capped mechanically by sandwiching titanium foil (5 μ m) with the graphite backing material and a stainless cover.

Table 1 summarizes the properties of the HSP and CONV sources. These sources have similar external shapes, whereas their backing materials are different.

3. Performance tests

A leak test was carried out in an ultra-high vacuum and no

E-mail address: maekawa.masaki@qst.go.jp (M. Maekawa).

<https://doi.org/10.1016/j.nimb.2020.08.001>

Received 15 June 2020; Received in revised form 22 July 2020; Accepted 8 August 2020
0168-583X/ © 2020 Elsevier B.V. All rights reserved.

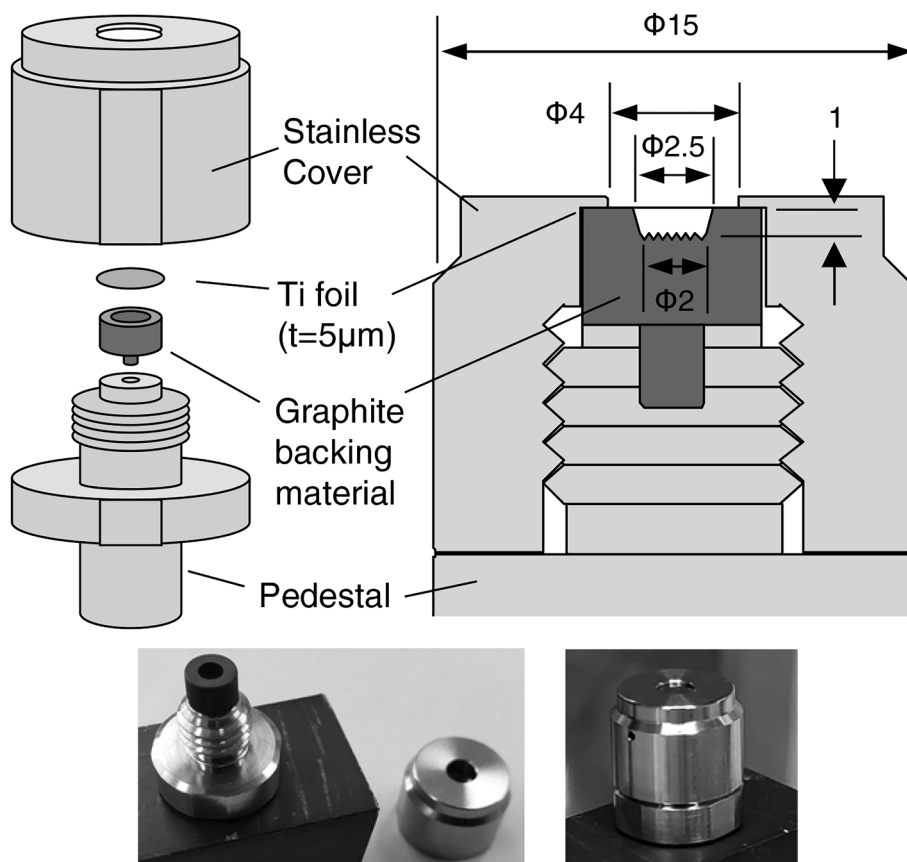


Fig. 1. Schematic of the positron source capsule fabricated in this work. Aqueous $^{22}\text{NaCl}$ solution is deposited into the tapered hole fabricated on the graphite backing material. The active area is sealed mechanically with Ti foil and a stainless cover. Units are in millimeters.

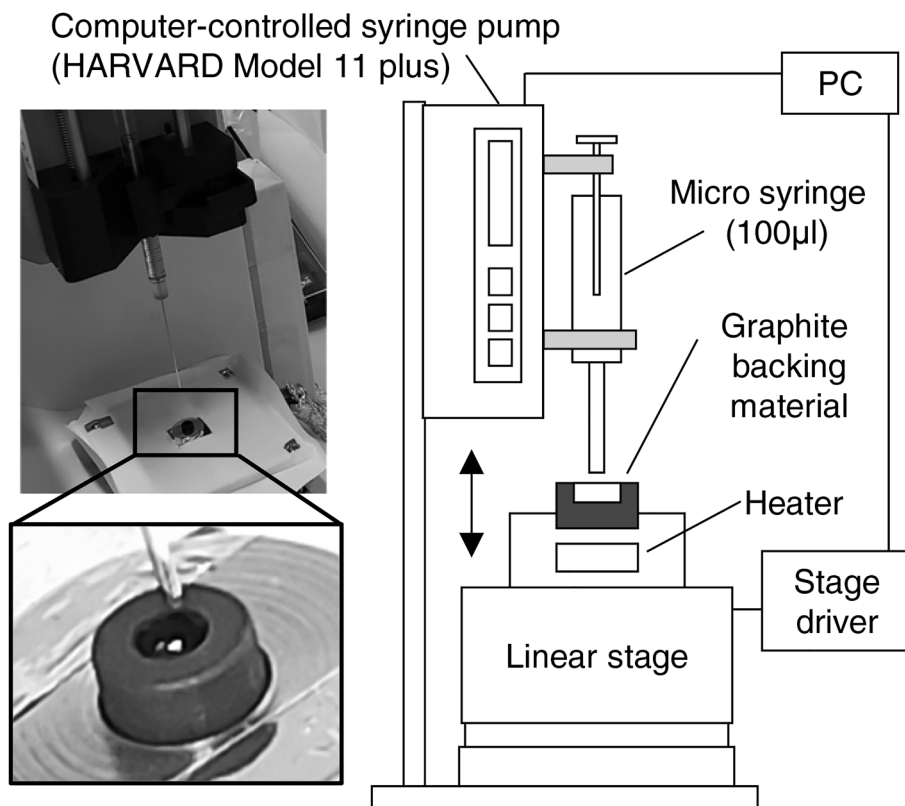


Fig. 2. Schematic of the source deposition system. An electric syringe pump is used to form 1 μL droplets of aqueous $^{22}\text{NaCl}$ solution, and the droplets are deposited individually into the hole on the graphite material.

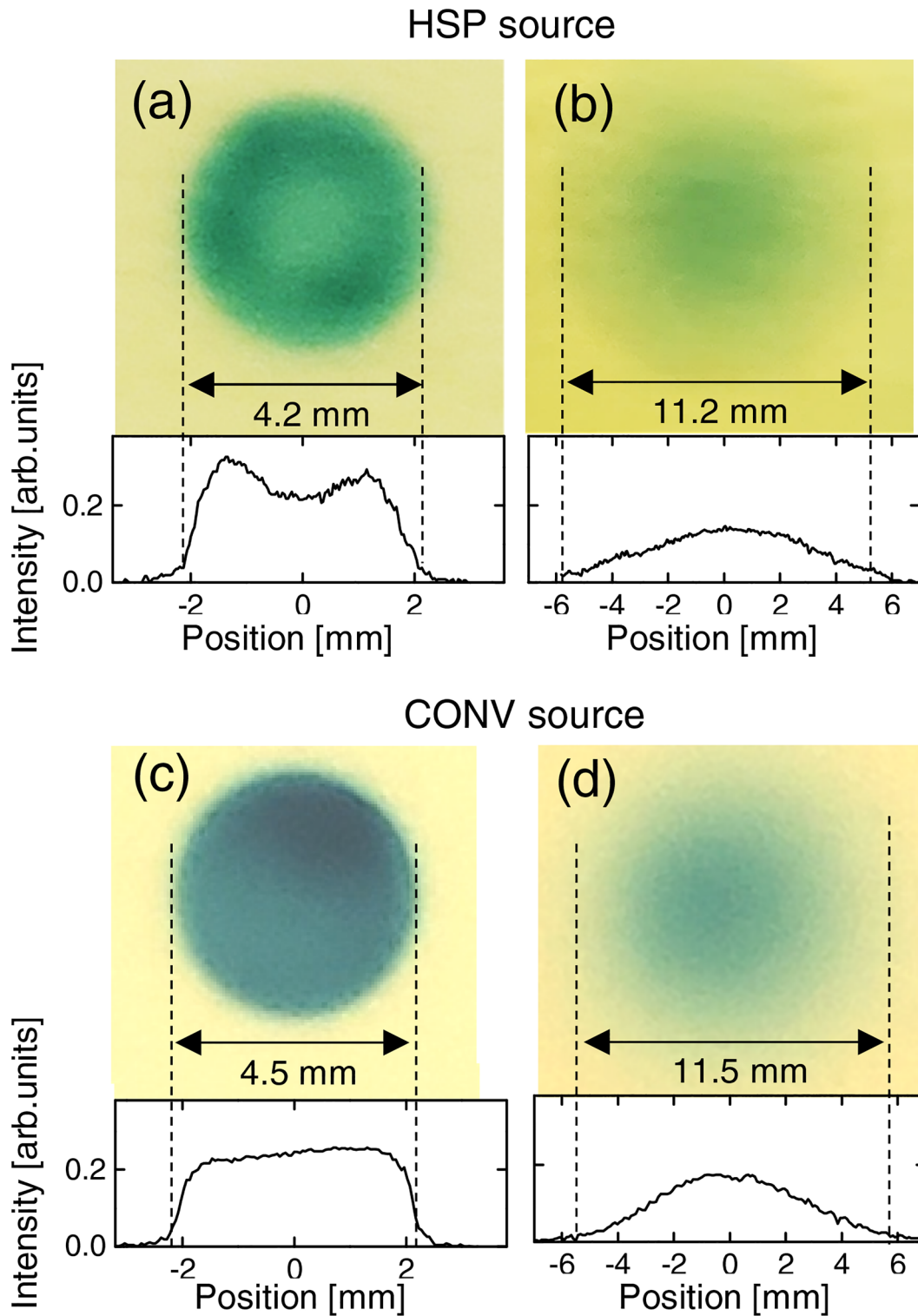


Fig. 3. Gafchromic film images of positrons and the intensities on the radius lines obtained for the (a) and (b) HSP and (c) and (d) CONV sources at the source exits ((a) and (c)), and 2 mm away from the source exits ((b) and (d)).

contamination was detected. This result confirmed that the source can be used for generating positron beams.

Using a radiochromic film (Gafchromic film, International Specialty Products Inc.) [26,27], the uniformity of the emitted positrons was observed immediately above and 2 mm from the source exit. A distance of 2 mm is the typical distance between the source and moderator in our positron beam apparatus. Exposure time was 5 and 150 min for the HSP and CONV sources, respectively.

The emission efficiency of positrons was determined by the slit-scan method (Fig. 4(a)). The number of annihilation gamma rays was counted through the lead slit that was 0.1 mm wide by a high-purity germanium (HPGe) detector that scanned the position of the source capsule. An aluminum plate was placed 2 mm above the source exit. The emission efficiency was obtained as the ratio of the annihilation gamma rays counts from the aluminum plate to the total counts.

The longitudinal spin polarization of the emitted positrons was

Table 1
Properties of the HSP and CONV sources.

Name	HSP (high spin polarization) self- assembled	CONV (conventional) commercial
Source amount	296 MBq	10 MBq
Backing material	graphite	tantalum
Deposited area diameter[mm]	$\phi 2.5$	$\phi 4$
depth[mm]	1	0.2
Source window material	titanium	titanium
thickness[μm]	5	5
diameter[mm]	$\phi 4$	$\phi 4$

determined through the magnetic field dependence of the S parameter related to the self-annihilation of spin-singlet positronium in $\alpha\text{-SiO}_2$ [28,29]. Fig. 5(a) shows the measurement system. The source capsule was buried in the electromagnet pole piece. The SiO_2 sample was set 2 mm from the source exit and only annihilation gamma rays from the sample were detected through the lead slit. The S parameters were determined from the DBAR spectra measured using the HPGe detector with an energy resolution of 1.4 keV at 511 keV. The details of the method have been described elsewhere [30].

In the system described above, magnetic Doppler broadening (MDB) measurements were carried out [9]. The MDB spectra were obtained as the difference of two DBAR spectra recorded at positive and negative magnetic fields with respect to the positron spin polarization [$N_+(p) - N_-(p)$]. The samples were well-annealed Fe and Cu polycrystals ($20 \times 20 \times 1$ mm). In each spectrum, more than 5×10^6 events were accumulated. All the spectra were normalized to the area

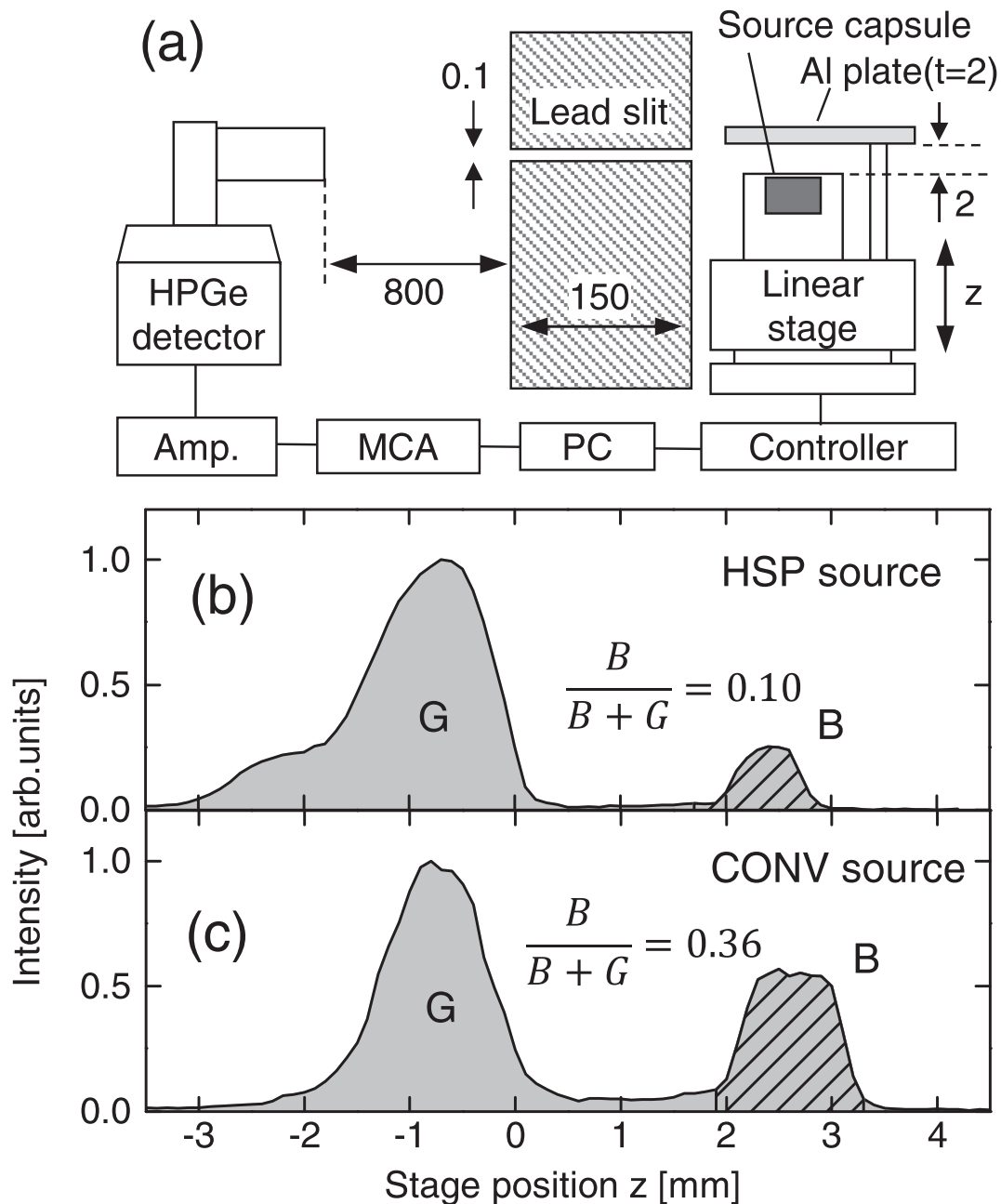


Fig. 4. (a) Schematic of the emission efficiency measurement system. Annihilation gamma rays are detected by the HPGe detector. The source position is changed by the linear motion stage. Intensities of annihilation gamma rays for the (b) HSP and (c) CONV sources.

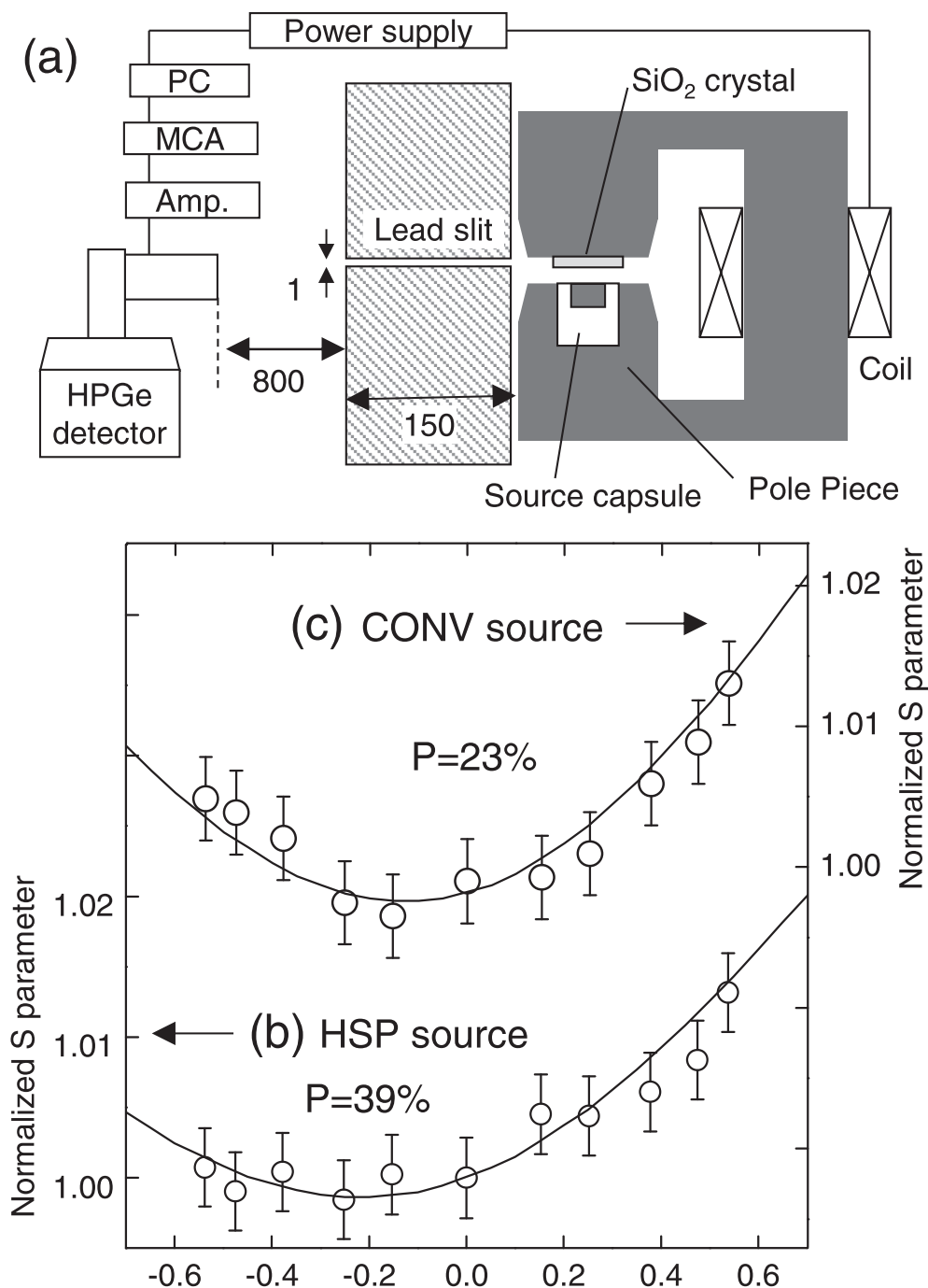


Fig. 5. Schematic of the spin polarization measurement system. The positron source is buried in the electromagnet pole piece. Magnetic field dependences of S parameters from α -SiO₂ obtained with the (b) HSP and (c) CONV sources. The curves are theoretical assuming appropriate spin polarizations.

intensities.

Finally, a slow positron beam with an energy of 12 keV was generated using the HSP and CONV sources and the electrostatic beam apparatus described elsewhere [31,11]. The beam profile was observed by a multichannel plate with a diameter of 10 mm. The beam intensity was also measured with the HPGe detector.

4. Results and discussion

4.1. Positron emission properties

Fig. 3 shows the spatial profiles of positrons emitted from the HSP and CONV sources obtained by the Gafchromic films at and 2 mm away

from the source exit. The CONV source exhibited a homogeneous positron profile at the source exit and a volcano-like profile 2 mm away from the source exit (Fig. 3(c) and (d)). In contrast, the HSP source showed a hollow profile at the source exit (Fig. 3(a)). This result indicated that some segregation of NaCl at the periphery of hole occurred despite its tapered shape and patterns on the bottom. Nevertheless, 2 mm away from the source exit, the hollow profile was averaged out and a volcano-like profile appeared, similar to the CONV source (Fig. 3(b)). Thus, the segregation effect did not affect the generation of positron beam as long as the source-moderator distance was appropriate.

Fig. 4(b) and (c) show the annihilation gamma ray intensities as a function of the relative distance between the source exit and the slit

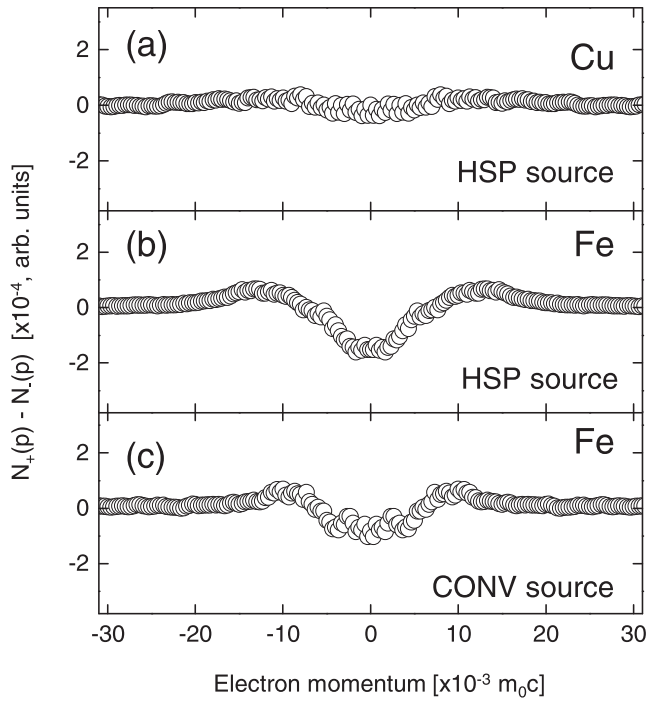


Fig. 6. MDB spectra obtained for the well-annealed Fe and Cu polycrystals in a magnetic field of 0.6 T with the (a) and (b) HSP source and (c) CONV source.

center obtained for the HSP and CONV sources. Here, for example, $z = 0$ means that the source exit is at the slit center. In either source, there were two major peaks, labeled G at $z \lesssim 0.5$ mm and B at $2 \lesssim z \lesssim 3$ mm. The G peak was due to the annihilation of positrons in the source

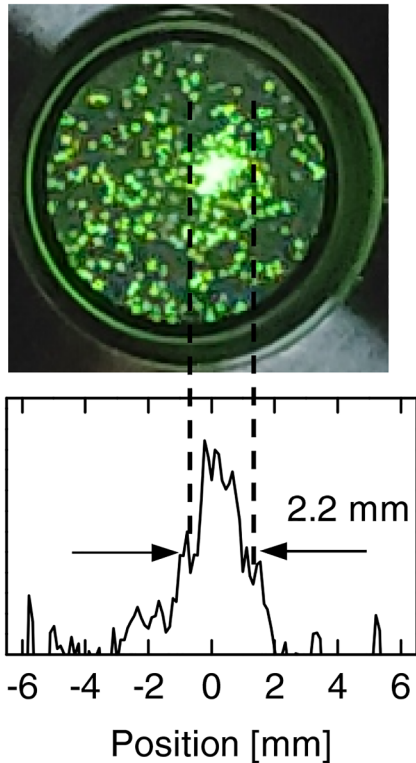
capsule. The peak B arose from the annihilation of positrons injected into the aluminum plate. For the HSP source, there was a large tail at $z \lesssim -2$ mm. This indicated that in the HSP source, more positrons penetrated the backing material (graphite) due to its lower density compared with the CONV source. The emission efficiency, f_{out} , is given by the intensity ratio of peak B to the total area. We obtained $f_{out} = 10\%$ for the HSP source and $f_{out} = 36\%$ for the CONV source. These efficiencies were substantially lower than 50%, which was expected from the positron emission in the 2π direction. To explain these efficiencies quantitatively, we need to consider not only the effect of back-scattering, but also the transmission of positrons through the source window and the multiple reflection of positrons between the source window and backing material, as discussed below.

Generally, the emission efficiency is given by

$$f_{out} = A \sum_n R_W^n R_B^n (1 - R_W)^n T,$$

where A is the effective solid angle of the source window, R_W and R_B are the reflectance of positrons by the source window and backing material, respectively, T is the transmittance of positrons through the source window, and n is the number of the reflection. The solid angle is given by $A = \frac{1}{2}(1 - a/\sqrt{r^2 + a^2})$, where r is the radius of the source area on the backing material and a is the relative distance from the source to the window. According to MacKenzie et al. [22], $R = 0.342 \log_{10} Z - 0.146$, where Z is the atomic number. The transmittance is given by $T = \exp(-\mu D t)$, where μ is the mass attenuation coefficient, D is the material density, and t is the thickness of the window. The mass attenuation coefficient is given by $\mu [m^2/kg] = 1.7 (E [MeV])^{-1.14}$, where E is the average positron energy ($E = 0.17$ [MeV]) [32]. For the HSP source, $A = 0.188$ with $r = 1.25$ mm, and $a = 1$ mm and $R_B = 0.12$ (graphite). For the CONV source, $A = 0.48$ with $r = 2$ mm and $a = 0.2$ mm and $R_B = 0.49$ (Ta). For both sources, $R_W = 0.313$ (Ti), $T = 0.714$ with the effective thickness of $t = 5.8$ μ m assuming the

(a) HSP source



(b) CONV source

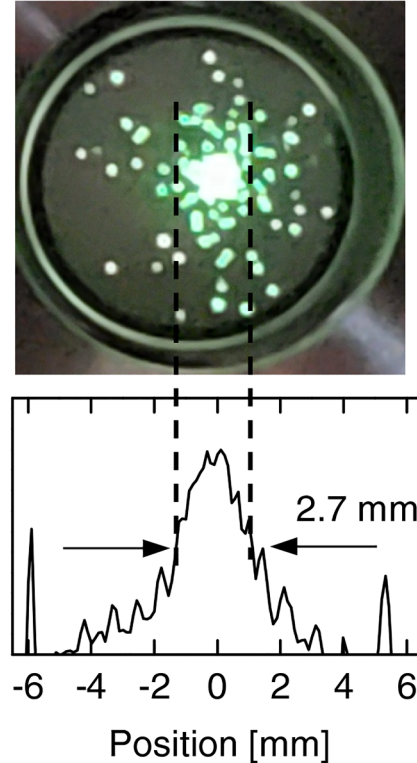


Fig. 7. Slow-positron beam images and cross-sectional profiles obtained for the HSP and the CONV sources.

average angle (60°) of positrons passing through the foil, and $D = 4.51 \text{ g/cm}^3$. Because R_W and R_B are below unity, it was sufficient to consider up to the second reflection ($n = 2$). Eventually, we found $f_{out} = 10\%$ for the HSP source and $f_{out} = 28\%$ for the CONV source. Thus, the emission efficiencies we obtained were roughly explained.

4.2. Spin polarization

Fig. 5 shows the S parameters as a function for the magnetic field obtained for the α -SiO₂ sample. By analyzing these data, the spin polarization was determined to be 39% for the HSP source and 23% for the CONV source. These values were lower than those estimated from $P_+ = (v/c)(1 + \cos\alpha)/2$ with the emission angles of $\alpha = 68.2^\circ$ for the HSP source and $\alpha = 87.2^\circ$ for the CONV source ($\alpha = \tan^{-1}(2r/a)$). The degradation of spin polarization was caused by including positrons backscattered by the backing material, as discussed below.

The spin polarization is generally given by $P = (N_\uparrow - N_\downarrow)/(N_\uparrow + N_\downarrow)$, where N_\uparrow and N_\downarrow are the numbers of up and down spins emitted in a direction, respectively. The numbers of up and down spins increased by backscattering are given by $N_\uparrow^{bs} = R_B \times N_\downarrow$ and $N_\downarrow^{bs} = R_B \times N_\uparrow$, respectively. The total polarization including the reflected positrons is given by

$$\begin{aligned} P_{tot} &= \frac{(N_\uparrow + N_\uparrow^{bs}) - (N_\downarrow + N_\downarrow^{bs})}{(N_\uparrow + N_\uparrow^{bs}) + (N_\downarrow + N_\downarrow^{bs})} \\ &= \frac{N_\uparrow - N_\downarrow}{N_\uparrow + N_\downarrow} \times \frac{1 - R_B}{1 + R_B} \\ &= P \times \frac{1 - R_B}{1 + R_B}. \end{aligned}$$

We found $P_{tot} = 38\%$ with $P = 48\%$ and $R_B = 0.12$ for the HSP source and $P_{tot} = 13\%$ with $P = 37\%$ and $R_B = 0.49$ for the CONV source. The observed spin polarization (39%) for the HSP source agreed well with this estimation, whereas that for the CONV source (23%) was higher. These results confirmed that suppressing the backscattered positrons was an effective method for increasing spin polarization.

Fig. 6 shows the MDB spectra obtained for the Fe and Cu samples. The amplitude was null in the Cu sample, whereas finite MDB amplitudes were observed in the Fe sample. This result indicated annihilation between spin-polarized positrons and electrons. The amplitude obtained with the HSP source was 1.7 times larger than that obtained with the CONV source, reflecting the difference in spin polarizations for these sources.

4.3. Slow positron beam generation

Fig. 7 shows the images of the slow positron beam generated with the HSP and CONV sources. The spot sizes were almost the same, although the intensity for the HSP source was 6 times greater than that for the CONV source, reflecting the difference in their source activities. Thus, we confirmed that the HSP source can be used for slow positron beam generation.

5. Conclusion

To obtain an HSP slow positron beam, a new positron source was fabricated using aqueous ²²NaCl solution and a graphite backing material. This source had sufficient sealing performance and was suitable for slow positron beam generation. The higher spin polarization of positrons emitted from this source will enable future studies of magnetic materials. A further advantage is that when the activity is lost, the

source can be recharged with additional. aqueous ²²NaCl solution

CRedit authorship contribution statement

Masaki Maekawa: Conceptualization, Methodology, Software, Investigation, Formal analysis, Writing - original draft, Writing - review & editing, Visualization. **Ken Wada:** Investigation, Validation. **Atsuo Kawasuso:** Writing - review & editing, Supervision, Project administration.

Declaration of Competing Interest

The authors declare that they have no known competing financial interests or personal relationships that could have appeared to influence the work reported in this paper.

References

- [1] P.W. Zitzewitz, J.C.V. House, A. Rich, D.W. Gidley, Phys. Rev. Lett. 43 (1979) 1281–1284.
- [2] A. Kawasuso, M. Maekawa, Appl. Surf. Sci. 255 (2008) 108–110.
- [3] P.G. Coleman, A. Kallis, J. Phys. Conf. Ser. 262 (2011) 012016.
- [4] D.W. Gidley, A.R. Köymen, T.W. Capehart, Phys. Rev. Lett. 49 (1982) 1779–1783.
- [5] A. Rich, J.V. House, D.W. Gidley, R.S. Conti, Appl. Phys. A 43 (1987) 275–281.
- [6] A. Rich, R.S. Conti, D.W. Gidley, M. Skalsey, J.V. House, P. Zitzewitz, Hyperfine Interactions 44 (1988) 125–138.
- [7] H. Li, M. Maekawa, A. Kawasuso, N. Tanimura, J. Phys. Condens. Matter 27 (2015) 246001.
- [8] H. Li, M. Maekawa, A. Miyashita, A. Kawasuso, Appl. Phys. Lett. 110 (2017) 172402.
- [9] A. Kawasuso, M. Maekawa, Y. Fukaya, A. Yabuuchi, I. Mochizuki, Phys. Rev. B 83 (2011) 100406(R).
- [10] A. Kawasuso, M. Maekawa, Y. Fukaya, A. Yabuuchi, I. Mochizuki, Phys. Rev. B 85 (2011) 024417.
- [11] A. Kawasuso, Y. Fukaya, M. Maekawa, I. Mochizuki, H. Zhang, J. Phys. Conf. Ser. 443 (2013) 012084.
- [12] M. Maekawa, H. Abe, A. Miyashita, S. Sakai, S. Yamamoto, A. Kawasuso, Defect Diffusion Forum 373 (2017) 65–70.
- [13] M. Maekawa, S. Sakai, A. Miyashita, A. Kawasuso, e-J. Surf. Sci. Nanotech. 16 (2018) 347–350.
- [14] A. Kawasuso, Y. Fukaya, M. Maekawa, H. Zhang, T. Seki, T. Yoshino, E. Saitoh, K. Takanashi, J. Mag. Mag. Mater. 342 (2013) 139–143.
- [15] H.J. Zhang, S. Yamamoto, Y. Fukaya, M. Maekawa, H. Li, A. Kawasuso, T. Seki, E. Saitoh, K. Takanashi, Sci. Rep. 4 (2014) 04844.
- [16] H.J. Zhang, S. Yamamoto, B. Gu, H. Li, M. Maekawa, Y. Fukaya, A. Kawasuso, Phys. Rev. Lett. 114 (2015) 166602.
- [17] A. Miyashita, M. Maekawa, K. Wada, A. Kawasuso, T. Watanabe, S. Entani, S. Sakai, Phys. Rev. B 97 (2018) 195405.
- [18] S.S. Hanna, R.S. Preston, Phys. Rev. 106 (1957) 1363–1364.
- [19] S. Berko, Positron annihilation in ferromagnetic solids, in: A.J. Stewart, L.O. Roellig (Eds.), Positron Annihilation, Academic Press, 1967, pp. 61–80.
- [20] R.S. Preston, S.S. Hanna, Phys. Rev. 110 (1958) 1406–1408.
- [21] L.A. Page, Rev. Mod. Phys. 31 (1959) 759–781.
- [22] I.K. MacKenzie, C.W. Shulte, T. Jackman, J.L. Campbell, Phys. Rev. A 7 (1973) 135.
- [23] V.A. Kuzminikh, S.A. Vorobiev, Nucl. Inst. Methods 167 (1979) 483.
- [24] J.A. Baker, P.G. Coleman, J. Phys. C 21 (1988) L875.
- [25] R. Krause-Rehberg, <http://positron.physik.uni-halle.de/source.html> (2002).
- [26] Y. Yuri, T. Ishizaka, T. Yuyama, I. Ishibori, S. Okumura, K. Yoshida, Nucl. Instr. Methods Phys. Res. A 642 (2011) 10.
- [27] T. Agetatsu, H. Hanaya, T. Kojima, Radioisotopes 57 (2008) 87 [in Japanese].
- [28] Y. Nagashima, T. Hyodo, Phys. Rev. B 41 (1990) 3937–3941.
- [29] Y. Nagai, Y. Nagashima, J. Kim, Y. Itoh, T. Hyodo, Nucl. Instr. Methods B 171 (2000) 199–203.
- [30] M. Maekawa, Y. Fukaya, A. Yabuuchi, I. Mochizuki, A. Kawasuso, Nucl. Inst. Meth. Phys. Res. B 308 (2013) 9–14.
- [31] A. Kawasuso, Y. Fukaya, M. Maekawa, A. Yabuuchi, J. Phys. Conf. Series. 225 (2010) 012028.
- [32] N. Tsoulfanidis, S. Landsberger, Measurement and detection of radiation, 4th edition, CRC Press, 2015 pp. 131.